**JOURNAL OF CURRENT RESEARCH IN SCIENCE (ISSN 2322-5009)**
**2013, Vol. 1, No. 3, pp:144-150**
**Available at www.jcrs010.com**

**ORIGINAL ARTICLE**

# NON FOURIER HEAT CONDUCTION IN A SEMI INFINITE BODY EXPOSED TO THE PULSATILE AND CONTINUOUS HEAT SOURCES

Mohammad Akbari*, Mohammad Hemmat Esfe, Seyed Hadi Rostamian, Arash Karimipour
*Department of Mechanical Engineering, Najafabad Branch, Islamic Azad University, Isfahan, Iran*

**ABSTRACT:** In this paper, the melting of a semi-infinite body as result of a continuous or pulsatile moving laser beam has been studied. It has been known that classical Fourier heat diffusion analyses fail to accurately model transient thermal responses in extremely high heat flux, low temperature, and high speed energy transport engineering applications because they assume that thermal energy transport is occurring at an infinite propagation speed. In addition, thermophysical properties such as heat conductivity coefficient, density and heat capacity are functions of temperature and material states. The enthalpy technique used for the solution of phase change problems in an explicit finite volume form for the hyperbolic heat transfer equation. This technique used to calculate the transient temperature distribution in the semi-infinite body and the growth rate of the melt pool. Temporal variation of laser beam intensity in two cases of continuous and pulsatile heat flux considered. In order to validate the numerical results, comparisons made with experimental data. Finally, the results of this paper compared with similar problem that has used the Fourier theory. The comparison shows the influence of infinite speed of heat propagation in Fourier theory on the temperature distribution and the melt pool size.
**KEYWORDS**: Non-Fourier, Enthalpy Technique, Melt Pool, Radiational Boundary Condition.

## INTRODUCTION

Investigation of melting and solidification phenomena is important in most heat transfer engineering problems. For instance, in semiconductors producing technology, welding, found, crystallization etc. The use of concentrated heat source energy such as laser and electrical discharge machining (EDM) are common nowadays in melting various materials. In all of problems like this, the solid and liquid phases are separated with an interface; interface developing in the solid or liquid phase, depends on both sides of the temperature gradients. Rostami and Russo, (1990) investigated the heating and melting of a semi-infinite body due to a stationary laser beam. Because the laser beam was stationary, the problem was assumed to be axisymmetric. The numerical solution was compared with experimental data and, because no vaporization occurred at the surface of the workpiece, reasonable agreement was seen.

Rostami and Raisi, (1997) studied the heating and melting of a semi-infinite body due to volumetric absorption of moving laser radiation. That was a transient three-dimensional conduction problem with a moving heat source and a moving phase boundary, which was used with an explicit finite difference method. Temperature distribution and melt pool size for moving and a stationary laser beam were derived. In order to validate, the numerical solution was compared with experimental data. The comparisons showed that the numerical results were accurate.

Sadd and Didlake, (2001) investigated the melting of a semi-infinite solid in one dimensional based on non-Fourier heat conduction law postulated by Cattaneo, (1986) and Vernotte, (1986). They confirmed that, unlike the classical Fourier theory, which predicts an infinite speed of heat propagation, the non-Fourier theory implied that the speed of a thermal distribution is finite, and the effect of this finite thermal wave speed on the melting phenomenon was determined. Finally, they found out that, non-Fourier results differ from the Fourier theory only for small values of time.

Tang and Araki, (1996a) have solved the problem of non-Fourier heat conduction in a finite medium under periodic surface disturbance. The periodic condition was a harmonic one. Mikhailov and Cotta, (1997) solved the steady-periodic hyperbolic heat conduction in a finite slab by the use of computer algebra system Mathematica. Abdel-Hamid, (1999) solved non-Fourier heat conduction under periodic surface disturbance using the finite integral transform. Tang and Araki, (1996b); Tang and Araki, (2000) investigated the non-Fourier heat conduction in a finite medium under pulse surface heating.

Jiang, (2002) investigated experiments on

**Corresponding Author:** Mohammad Akbari, Department of Mechanical Engineering, Najafabad Branch, Islamic Azad University, Isfahan, Iran. **E-mail:** m.akbari.g80@gmail.com

porous material heated by a microsecond laser pulse and the corresponding theoretical analysis. Some non-Fourier heat conduction phenomena were observed in the experimental sample. The experimental results indicated that only if the thermal disturbance be strong enough (i.e., the pulse duration is short enough and the pulse heat flux is great enough) it is possible to observe apparent non-Fourier heat conduction phenomenon in the sample, and evident non-Fourier heat conduction phenomenon can only exist in a very limited region around the thermal disturbance position.

Abdel-Jabbar *et al.*, (2003) investigated the thermal behavior of a thin slab under the effect of a fluctuating surface thermal disturbance, as described by the dual-phase-lag heat conduction model. It has found that, using the dual-phase-lag heat conduction model is essential at large frequencies of the surface disturbance. Mathematical criteria that specify the limits, beyond which both the hyperbolic wave and the dual-phase-lag heat conduction models deviate from the diffusion models were obtained.

Ahmadikia and Rismanian, (2011) obtained the analytical scheme in solving the hyperbolic heat conduction in the fin that subjected to every periodic boundary condition using the Laplace transform method. Their results obtained from the hyperbolic heat conduction model successfully explained the non-Fourier thermal wave behavior in the small fin for fast phenomenon (high frequency periodic boundary condition). Ahmadikia *et al.*, (2012) analytically solved the Pennes bioheat transfer models by employing the Laplace transform method for small and large values of reflection power (albedo) during laser irradiation. They concluded that the non-Fourier effect should be considered during laser heating with low albedo, because errors in the predicted temperature values may occur.

## FORMULATION OF THE PROBLEM

A review of literatures indicated that all of the previous studies of the change-of-state heat transfer problems were based on the Fourier heat conduction law.

$$q = -k\nabla T \tag{1}$$

Equation (1) along with the conservation of energy gives the classical parabolic heat equation:

$$a\nabla^2 T=\frac{\partial T}{\partial t} \tag{2}$$

Many of the investigations indicated that Fourier's model possesses several serious shortcomings. The most prominent is that, this model implicates an infinite speed of heat propagation. Cattaneo and later Vernotte postulated a wave model for heat conduction in solids in the form below:

$$\tau\frac{\partial q}{\partial t}+q_x = -k\nabla T \tag{3}$$

The quantity $\tau$ is called the material thermal relaxation time and is a physical result of a finite thermal communication time between material points.

The conservation energy equation is given by:

$$q_x = q_{x+dx} + \frac{\partial}{\partial t}(\rho\rho cT)d \tag{4}$$

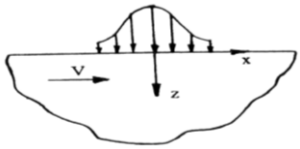


**Figure 1**: Schematic representation of the problem in the two-dimensional case.

Finally, by using Cattaneo combination and conservation of energy equations, hyperbolic heat transfer equation may be expressed as:

$$\frac{\partial(\rho\rho cT}{\partial t}+\tau\frac{\partial^2(\rho\rho cT}{\partial t^2}+V\frac{\partial(\rho\rho cT}{\partial x}=\frac{\partial}{\partial x}(k\frac{\partial T}{\partial x})+\frac{\partial}{\partial y}(k\frac{\partial T}{\partial y})+\frac{\partial}{\partial z}(k\frac{\partial T}{\partial z})+g \tag{5}$$

The corresponding volumetric heat generation is given by (1990):

$$g=-\frac{dI_a}{dz}=\alpha I_S(1-R)e^{-\alpha z} \tag{6}$$

Figure 1 shows a schematic of semi-infinite body. Profile of the beam is considered circular and elliptical. The intensity of the beam that has Gauss' distribution may be expressed as (Raisi, 1997):

$$I_S(x,y,t)=I_0 h(t) e^{-\left[(x^2+y^2)/w^2\right]} \tag{7}$$

$$I_S(x,y,t)=I_0 h(t) e^{-\left[(x/w_x)^2+(y/w_y)^2\right]} \tag{8}$$

In last equations, $w$ is the beam radius in the circular profile state; $w_x$ and $w_y$ are the beam radius in the x and y directions, in elliptical profile state. $I_0$ is the radiation intensity at the center of the beam, and *h(t)* stands for the temporal variation of the intensity. In the case of continuous heat flux, *h(t)* has the constant value of unity, whereas in the pulsatile case it varies with time according to the following equation:

$$\begin{cases} h(t)=\frac{1}{2}\Delta t-\frac{5}{2}(n-1) & \text{if} \quad 5(n-1)\Delta)\le t\le(5n-3)\Delta)\Delta t \quad n=1,2,3,\ldots \\ h(t)=-\frac{1}{2}\Delta t+\frac{(5n-1)}{2} & \text{if} \quad (5n-3)\Delta)\le t\le(5n-1)\Delta) \\ h(t)=0 & \text{if} \quad (5n-1)\Delta)\le t\le 5n \end{cases} \tag{9}$$

The temporal variation of *h(t)* in pulsatile case, according to the above relation, is shown in Figure 2.

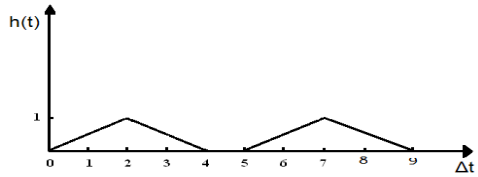


**Figure 2:** Variation of *h(t)* with respect to the time in pulsatile case.

The local intensity of radiation decreases inside the material according to:

$$I_a = I_S(1-R)\,e^{-\alpha z} \qquad (10)$$

Where R is the surface reflectivity and α is the absorption coefficient of the material.

Equation (5) must be solved for the solid and liquid phase separately. The two solutions should then be related via the energy boundary conditions at the solid-liquid interface. The dependence of the position of the interface on the temperature distribution makes the problem complicated. One way to avoid this complexity is to write the left side of Equation (5) in terms of enthalpy:

$$\frac{\partial e}{\partial t}+\tau\frac{\partial^2 e}{\partial t^2}+V\frac{\partial e}{\partial x}=\frac{\partial}{\partial x}(k\frac{\partial T}{\partial x})+\frac{\partial}{\partial y}(k\frac{\partial T}{\partial y})+\frac{\partial}{\partial z}(k\frac{\partial T}{\partial z})+g \qquad (11)$$

In Equation (11) *e* is term of enthalpy and may be expressed as:

$$e = \int \rho c\,dT \qquad (12)$$

*2.1. Initial and Boundary Conditions*

Initially, the temperature is equal to $T_i$ everywhere:

$$\text{at } t=0: \quad T=T_i \qquad (13)$$

Initially, the temperature variation is equal to zero

$$\text{at } t=0: \quad \frac{\partial T}{\partial t}=0 \qquad (14)$$

The boundary condition at the surface may be expressed as:

$$\text{at } z=0: \quad -k\frac{\partial T}{\partial z}=\varepsilon(T)\sigma(T^4-T_\infty^4)+h(T-T_\infty) \qquad (15)$$

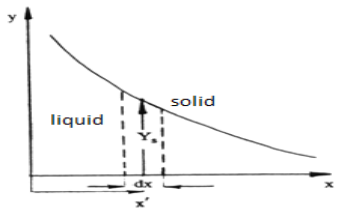


**Figure 3:** Solid-Liquid interface in a two-dimensional view.

Regions far from the source are supposed to be uninfluenced by the source:

$$\begin{aligned}&\text{at } x\to\pm\infty: \quad T=T_i\\ &\text{at } y\to\pm\infty: \quad T=T_i\end{aligned} \qquad (16)$$

*2.2 Conditions at the Interface*

The energy balance at the interface is shown in figure 3 may be written as (Raisi, 1997):

$$\begin{aligned}&\left[1+(\frac{\partial X_s}{\partial y})^2+(\frac{\partial X_s}{\partial z})^2\right]\left[k_s\frac{\partial T_s}{\partial x}-k_\ell\frac{\partial T_\ell}{\partial x}\right]=L(\tau\frac{\partial^2 X_s}{\partial t^2}+\frac{\partial X_s}{\partial t}-V)\\ &\left[1+(\frac{\partial Y_s}{\partial x})^2+(\frac{\partial Y_s}{\partial z})^2\right]\left[k_s\frac{\partial T_s}{\partial y}-k_l\frac{\partial T_\ell}{\partial y}\right]=L(\tau\frac{\partial^2 Y_s}{\partial t^2}+\frac{\partial Y_s}{\partial t})\\ &\left[1+(\frac{\partial Z_s}{\partial x})^2+(\frac{\partial Z_s}{\partial y})^2\right]\left[k_s\frac{\partial T_s}{\partial z}-k_\ell\frac{\partial T_l}{\partial z}\right]=L(\tau\frac{\partial^2 Z_s}{\partial t^2}+\frac{\partial Z_s}{\partial t})\end{aligned} \qquad (17)$$

Where $X_s$, $Y_s$, $Z_s$ indicate the coordinates of the interface in the x, y and z directions, also $\frac{\partial X_s}{\partial t}$, $\frac{\partial Y_s}{\partial t}$, $\frac{\partial Z_s}{\partial t}$ are the velocity components of the interface in the x, y, and z directions, respectively. Once the enthalpy of each element is calculated, the following relations can be used to obtain the corresponding temperature (Rostami *et al.*, 1992):

$$\begin{aligned}&e_s=\int_{Tms}^{T}\rho_s c_s dT && T_{ms}\le T\\ &e_l=\int_{T_{ml}}^{T}\rho_l c_l\,dT+L && T_{ml}\ge T\end{aligned} \qquad (18)$$

$e_s$, $e_l$ are the amounts of the enthalpy in solid and liquid phases, respectively.

When an element contains both phases, x (i.e., the volume fraction of the liquid phase) must be calculated initially. The average enthalpy can be calculated afterward.

$$e=xe_l+(1-x)e_s \qquad (19)$$

A procedure for the evaluation of the liquid fraction x will be introduced later.

For $\rho c$ an average value was assumed and by substitution $e_s$, $e_l$ from Equation (18) in Equation (19), Equation (20) can be written as follow:

$$e=xL+(\rho\rho c_{av}(T-T_m)) \qquad (20)$$

Where, $T_m$ is melt temperature.

## THERMOPHYSICAL PROPERTIES

The thermophysical properties of the material were allowed to vary with temperature and phase state of the material. These properties for unalloyed aluminum may be expressed as (Touloukian, 1972; Rohsenow, 1985)

*3.1 Thermal Conductivity Coefficient* $K(\frac{W}{m^\circ k})$

$$\begin{aligned}&K_s=226.67+0.033T && 300K<T\le 400K\\ &K_s=226.6-0.055T && 400K<T\le 933K\\ &K_s=63+0.03T && 933K<T\le 1600K\\ &K_s=114 && 1600K\le T\le 2723K\end{aligned} \qquad (21)$$

*3.2 Specific Heat at Constant Pressure* $C_p(^{kj}/_{kgk})$

$$\begin{aligned}&cp_s=0.762+4.67\times10^{-4}T && 300K<T\le 933K\\ &cp_1=0.921 && T>933K\end{aligned} \qquad (22)$$

*3.3 Density* $\rho(kg/m^3)$

$$\rho_s = 2767 - 0.22T \qquad 300K < T \le 933K \tag{23}$$

*3.4 Emissivity Coefficient* $\varepsilon$

$$\varepsilon = 7.2\times10^{-5}T + 3.2\times10^{-3} \tag{24}$$

Also, latent heat of diffusion is equal to:

$$L = 3.95\times10^{5} \ J/kg \tag{25}$$

By using these equations, $e_s$, $e_l$ may be expressed as two polynomial functions in order 3 and 2, respectively.

$$e_s = 2108.454T + 0.5622T^2 - 3.4246\times10^{-5}T^3 - 2428827.8$$
$$e_l = 2431.44T + 0.12663T^2 + 9.4\times10^{8} \tag{26}$$

$(\rho c)_{av}$ can be expressed as:

$$(\rho\rho c_{av} = x(\rho(\rho_l + (1-x)(\rho)(_s \tag{27}$$

Which $(\rho c)_s$ and $(\rho c)_l$ are related to solid and liquid states, respectively.

By substituting Equation (27) in Equation (20), Equation (20) can be written as follow:

$$e = xL + (306822 - 87309x)(T - T_m) \tag{28}$$

In the numerical solution when an element contains only solid phase, the temperature can be calculated by applying the first term of Equation (26), using the Newton-Raphson method. On the other hand, when an element contains only liquid phase, the temperature can be calculated by solution of polynomial function of order 2 in second term of Equation (26). If an element contains two phases, Equation (28) can be utilized to calculate the temperature.

## NUMERICAL SOLUTION

In order to save computation time, the solution domain was divided into two regions: The inner region, which contains the liquid and/or solid state and the outer region, containing only the solid state. A fine mesh was used for the inner region, where the temperature gradients are large and the solid-liquid interface is present. The dimensions of the inner domain are smaller than outer region. Based on the work of Kou et al., (1981) $I_0 w$ is an important parameter. If $I_0 w < 1\times10^6$, the maximum temperature in the workpiece will not reach the boiling point of aluminum. Under this condition the maximum diameter of the melt pool is approximately $2.4w$ and depth of melt pool is nearly $w$ for a stationary beam. In numerical solutions often beam radius is considered about 100μm. Based on these arguments, the diameter of the inner region will be 240 microns (μm). However, because of moving heat source it was chosen to be 300 microns. The outer boundary of the computation domain was chosen such that conditions at infinity could be applied. The outer region radius usually is considered as 20 times of the beam radius. Then for a beam with a radius of 100 μm the $R_0$ can be calculated as follow:

$$R0 = 20\times w = 2000\ \mu m \tag{29}$$

For determining the number of grids in the inner region, the grid study was used. First, the temperature of central point of body geometry versus the grid numbers was drawn in figure 4. The results showed that temperature changing in 15th grid and higher can be assumed uniform and can be neglected. As a result, the grid numbers in inner region were considered as 15×15.

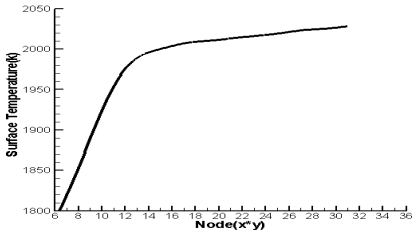


**Figure 4:** Temperature variation of the surface central point versus number of the nodes.

Grid numbers in z direction considered as 13. Hence:

$$\Delta x_i = \Delta y_i = \frac{300}{15} = 20\mu0 \ , \ \Delta z_i = 12\mu2 \tag{30}$$

Each 5 internal grids are equivalent to one external grid. Therefore:

$$\Delta x_o = \Delta y_o = 5\times\Delta x_i = 100\mu0 \ , \ \Delta z_\circ = 5\times\Delta z_i = 60\mu0 \tag{31}$$

Finally, (15 ×15 ×13 = 2925) rectangular grids were used for the inner region, and 57127 grids for outer region (figure 5).

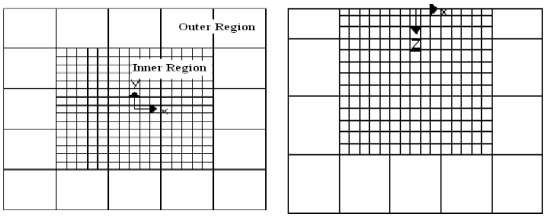


**Figure 5:** Grid generation in x-y and x-z planes.

## RESULTS AND DISCUSSION

In numerical solution of Equation (11) in explicit finite volume form, the beam intensity was $I_0 = 3.5\times10^9 \left(W/m^2\right)$, the target velocity $Vw/2\alpha = 0.45$, relaxation time $\tau = 0.2\times10^{-14}$sec

([Ashcroft *et al.*, 1972](#)) and the beam radius was 100μm. A pulse duration of $t_{p=}1ms$ was used and initial temperature was 300K.

Figure 6 shows the maximum depth of the melt pool as a function of the beam intensity. It is assumed that the surface absorbs all of the beam energy. As it can be seen from Figure 6, the numerical analysis is in good agreement with the experimental data, for low beam intensity. However, in the wake of the reaching to the vaporization threshold, the numerical analysis and experimental data are becoming further from each other.

Figure 7 shows the depth of the melt pool as a function of the radius distance from the center of the beam. In this Figure, it can be seen that, there is negligible difference between numerical analysis and experimental data.

The temperature distribution of the center point as a function of time at various velocities is shown in Figure 8. As it observed, as much as the velocity of the beam increases, the temperature of the point decreases. This phenomenon is observed, due to the fact that as much as the velocity increases, the amount of energy that the specific point observes decreases.

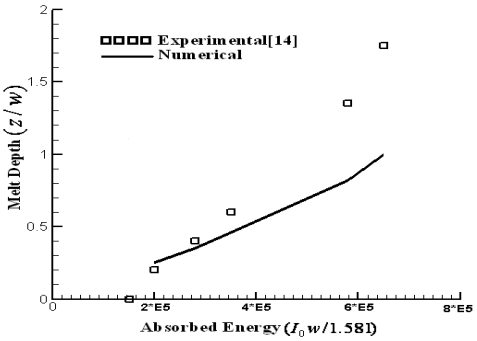


**Figure 6:** Melting pool depth versus laser beam intensity at the center.

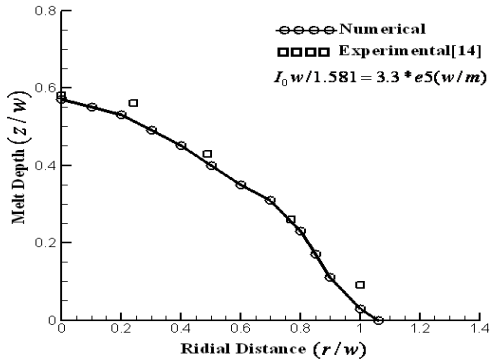


**Figure 7:** Melting pool depth versus radial distance from the laser beam center.

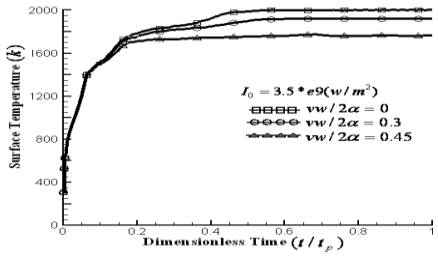


**Figure 8:** Surface center point temperature with respect to the time at various speeds and intensity of $I_0=3.5\times10^9\left(W/m^2\right)$ in continuous heat flux case.

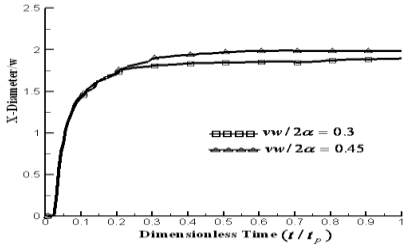


**Figure 9:** Melting pool diameter on the x-axis with respect to the time for two different speeds in continuous heat flux case.

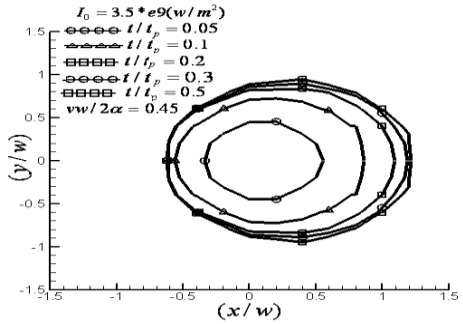


**Figure 10:** Melting pool image on the x-y plane at a constant velocity and different times for a circular laser beam in continuous heat flux case.

Figure (9) shows the diameter of the melt pool along x direction at z=0. It can be seen that, as much as the velocity of the beam increases, the diameter of the melt pool along x direction increases slightly. On the other hand, by increasing the velocity of the beam, the diameter of the melt pool along y direction decreases.

The solid-liquid boundary of the melt pool in the xy plane for $v_{w/2\alpha=0.45}$ is shown in Figure 10. It can be perceived from Figure 10 that, because of the moving beam, the melt pool tends to the right. In addition, as time passes, the diameter of the melt pool increases and eventually it reaches to a specific value.

Figure 11 shows the solid-liquid boundary of the melt pool in xz plane for $Vw/2\alpha=0.3$. Due to the moving beam, the melt pool tends to the right.

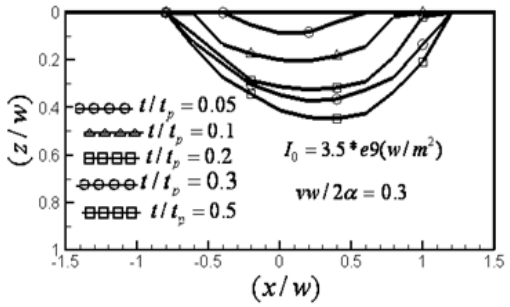


**Figure 11:** Melting pool image on the x-z plane at a constant velocity and different times for a circular laser beam in continuous heat flux case.

Also, the diameter of the melt pool along x direction at z=0 for dimensionless velocity $Vw/2\alpha=0.45$, is shown in Figure 12. It can be seen from this Figure that, the diameter of the melt pool along x direction, using Fourier model, can increases faster and finally it reaches to a specific value.

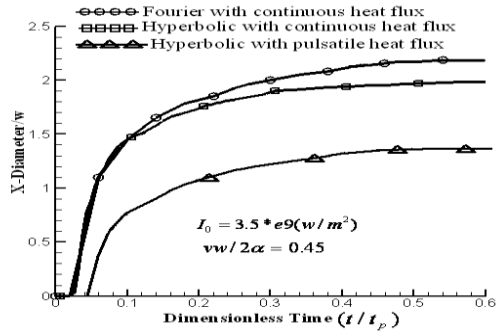


**Figure 12:** Melting pool diameter on the x-axis versus time using Fourier and Hyperbolic methods.

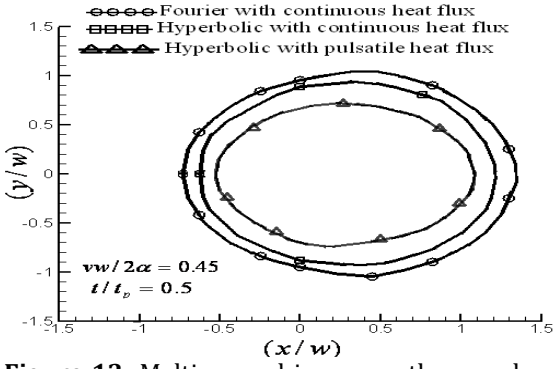


**Figure 13:** Melting pool image on the x-y plane for a circular laser beam using Fourier and Hyperbolic methods.

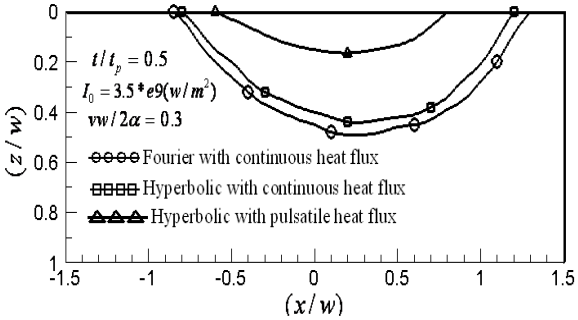


**Figure 14:** Melting pool image on the x-z plane for a circular laser beam using Fourier and Hyperbolic methods.

The solid-liquid boundary in xy plane at $\frac{t}{t_p}=0.5$ for $Vw/2\alpha=0.45$ is shown in Figure 13. As it can be predicted from Figure 12, the size of the melt pool in xy plane when Fourier model is used is greater than when the hyperbolic model with continuous and pulsatile heat flux is used.

Figure 14 shows the solid-liquid boundary of the melt pool in xz plane at $\frac{t}{t_p}=0.5$ for $Vw/2\alpha=0.45$.

According to Figure 14 it can be concluded that, using Fourier model, the size of the melt pool in xz plane is greater than the same melt pool obtained from the hyperbolic model in the two continuous and pulsatile cases.

## CONCLUSION

The temperature distribution and the size of the melt pool for an aluminum solid under the laser beam were studied. The hyperbolic heat equation was applied. The results of the hyperbolic model and the Fourier model were compared and it was seen that the increment of the melt pool and temperature fields were slower, when the hyperbolic model in continuous and pulsatile cases was applied. This phenomenon is in the wake of the infinite speed of the thermal waves in Fourier model. Also it was deduced that, the hyperbolic heat conduction model is suitable for short times and large domains and it can reached to the accurate results. In general, in practical applications such as electrical discharge machining (EDM), the pulsatile model has a better effectiveness than Fourier and continuous hyperbolic models.

## ACKNOWLEDGMENT

The authors gratefully acknowledge the support of the department of mechanical engineering and the office of gifted of Najafabad University for funding the current research grant.

## REFERENCES

Abdel-Hamid B. Modelling non-Fourier heat conduction with periodic thermal oscillation using the finite integral transform. Appl Math Model 1999;23:899–914.

Abdel-Jabbar NM, Nimr MA. The Dual phase-lag heat conduction model in thin slab under fluctuating thermal disturbance. Heat Transfer Engineering 2003;24:47-54.

Ahmadikia H, Rismanian M. Analytical solution of non-Fourier heat conduction problem on a fin under periodic boundary conditions. Journal of Mechanical Science and Technology 2011;25:2919-2926.

Ahmadikia H, Moradi A, Fazlali R, Basiri Parsa A. Analytical solution of non-Fourier and Fourier bioheat transfer analysis during laser irradiation of skin tissue. Journal of Mechanical Science and Technology 2012;26(6):1937-1947.

Ashcroft N, David N. Solid State Physics 1975; PP: 10.

Cattaneo C. A Form of conduction Equation which eliminates the Paradox of Instantaneous Propagation. Compt Rend 1986;247:431-442.

Jiang F. Non-Fourier heat conduction phenomena in porous material heated by microsecond laser pulse. Taylor & Francis 2002;6:331-346.

Kou S, Hsu SC, Mehrabian R. Rapid melting and solidification of a surface due to a moving heat flux. Metallurgical Trans Metallurgical Transactions B 1981;12(1):33-45.

Mikhailov MD, Cotta RM. Steady-periodic hyperbolic heat conduction in a finite slab. Int Commun Heat Mass Transfer 1997;24:725–731.

Raisi A. Calculation of the temperature field and the melt pool shape due to laser heating (in Farsi), M.S. thesis. Isfahan University of technology, Isfahan, Iran 1997.

Rohsenow WM, Hartnett JP. Handbook of heat transfer fundamentals. McGraw Hill, New York 1985; chapter 3.

Rostami AA, Russo RE. Unsteady two-dimensional heat transfer in laser heated materials. Processing in Transport phenomena in Material. ASME Publication HID 1990;pp:146.

Rostami AA, Raisi A. Temperature distribution and melt pool size in a semi-infinite body due to a moving laser heat source. Numerical Heat transfer 1997;31:783-796.

Rostami AA. Greif R, Russo RE. Modified Enthalpy Method Applied to Rapid melting and solidification. Int J Heat Mass Transfer 1992;35:2161-2172.

Sadd MH, Didlake JE. Non-Fourier melting of a same infinite solid. J Heat Transfer 2001;81:25-28.

Tang DW, Araki N. Analytical solution of non-Fourier temperature response in a finite medium under laser-pulse heating. Heat Mass Transf 1996a;31:359–363.

Tang DW, Araki N. Non-Fourier heat conduction in a finite medium under periodic surface thermal disturbance. Int J Heat Mass Transf 1996b;39:1585–1590.

Tang DW, Araki N. Non-Fourier heat conduction behavior in finite mediums under pulse surface heating. Mat Sci Eng A 2000;292:173–178.

Touloukian YS, Ho CY. Thermophysical properties of Matters. New York, plenum press1972;1-4.

Vernotte P. Paradox in the Continuous Theory of Heat Equation. Compt Rend 1986;246:3154-3159.